

Warming temperatures lead to reduced summer carbon sequestration in the U.S. Corn Belt

Zhongjie Yu ^{1,3}, Timothy J. Griffis ¹ & John M. Baker^{1,2}

The response of highly productive croplands at northern mid-latitudes to climate change is a primary source of uncertainty in the global carbon cycle, and a concern for future food production. We present a decadal time series (2007 to 2019) of hourly CO₂ concentration measured at a very tall tower in the United States Corn Belt. Analyses of this record, with other long-term data in the region, reveal that warming has had a positive impact on net CO₂ uptake during the early crop growth stage, but has reduced net CO₂ uptake in both croplands and natural ecosystems during the peak growing season. Future increase in summer temperature is projected to reduce annual CO₂ sequestration in the Corn Belt by 10–20%. These findings highlight the dynamic control of warming on cropland CO₂ exchange and crop yields and challenge the paradigm that warming will continue to favor CO₂ sequestration in northern mid-latitude ecosystems.

¹Department of Soil, Water, and Climate, University of Minnesota-Twin Cities, St. Paul, MN, USA. ²Agricultural Research Service, US Department of Agriculture, St. Paul, MN, USA. ³Present address: Department of Natural Resources and Environmental Sciences, University of Illinois Urbana-Champaign, Urbana, IL, USA. email: zjyu1986@gmail.com; timgriffis@umn.edu

Atmospheric carbon dioxide (CO₂) contributes to climate change through its impact on the Earth's radiation budget¹. Atmospheric CO₂ concentration has increased at an unprecedented rate from 280 ppm at the start of the industrial revolution to over 400 ppm in recent years, arising primarily from the burning of fossil fuels². Not all CO₂ emitted from anthropogenic sources remains in the atmosphere; about one-fourth of the emissions are currently absorbed by the terrestrial biosphere³, which has significantly slowed down global warming⁴. Unlike the anthropogenic emissions, the terrestrial carbon (C) sink is driven by two large opposing ecosystem fluxes, i.e., photosynthesis and respiration, and is often indirectly estimated from the residuals of global C budgets. This results in large uncertainties regarding the magnitude and distribution of this terrestrial C sink across spatial and temporal scales⁵.

While it is challenging to precisely quantify the terrestrial C sink strength, trends and variations in atmospheric CO₂ concentration provide a unique lens through which to probe the dynamics of the terrestrial C cycle as well as its interactions with climate. There is wide recognition that the amplitude of the seasonal oscillation of atmospheric CO₂ (i.e., annual peak-to-trough difference in atmospheric CO₂ concentration) in the northern hemisphere has increased by ~50% since the 1960s, tracking the pace of the contemporary climate warming^{6,7}. A feature of this increase in the CO₂ seasonal amplitude is a progressively earlier and larger drawdown of atmospheric CO₂ concentration in northern spring and summer, indicating warming-driven lengthening and intensification of photosynthetic activity in northern terrestrial ecosystems^{3,8}, in line with a widespread “greening” trend during the early 1980s to late 1990s^{9,10}. While this positive warming impact on terrestrial C uptake can be traced back to the 1980s, there is emerging evidence that the interannual correlations between growing season temperatures and CO₂ drawdown anomalies have been substantially attenuated or even reversed in direction at Mauna Loa¹¹ and northern high latitudes^{12–14} in recent decades. Although the underlying causal mechanisms remain unclear, these changing relationships appear to signal an emergent shift in both phase and magnitude of the terrestrial C sink and underscore a pressing need to better understand how C exchange dynamics is responding to ongoing climate change across a diverse range of northern terrestrial ecosystems¹⁵.

Though much research has focused on the C source and sink activities of tropical and boreal forest ecosystems, less attention has been paid to the role of terrestrial ecosystems at northern temperate latitudes (30° to 50° N) in the context of the global CO₂ seasonal cycle¹⁶. Previous studies showed that recent warming has resulted in altered phenology and increased net primary productivity (NPP) in spring and autumn in temperate forest ecosystems, suggesting a current and possible future enhancement of C sequestration in these ecosystems^{17,18}. Importantly, at northern mid-latitudes, terrestrial ecosystems are spatially heterogeneous and include a substantial area of croplands¹⁹. We know from a network of ecosystem-scale CO₂ exchange measurements^{20,21} and satellite observations²² that densely vegetated croplands have shorter but more intense C uptake periods than natural ecosystems and are one of the most productive systems on planet earth. Based on top-down and bottom-up models, Gray et al.²³ and Zeng et al.²⁴ argued that the intensification of agriculture at northern temperate latitudes was a major, yet largely overlooked, driver of changes in the CO₂ seasonal cycle of the northern hemisphere during the past five decades, accounting for 17–45% of the enhanced C exchange needed to explain the increasing CO₂ seasonal amplitude. Corn alone constitutes about two-thirds of this agricultural forcing, owing mostly to increasingly concentrated corn production in the

Midwestern United States (i.e., the U.S. Corn Belt) and northern China^{23,24}. However, due to the scarcity and limited time period of direct observations, considerable uncertainties remain with respect to the overall strength of this agricultural forcing and the extent to which heterogeneous terrestrial ecosystems at northern mid-latitudes will respond to future climate warming¹¹.

Here we present a decadal record (2007–2019) of direct boundary layer CO₂ measurements from a very tall tower in southern Minnesota (the University of Minnesota tall tower Trace Gas Observatory (KCMP)) (Fig. S1a) – a heterogeneous agricultural region that typifies the Corn Belt^{25–27}. We compared this decadal record with other long-term time series (2007–2018) of atmospheric CO₂ data within the U.S. Midwest (i.e., Park Falls, Wisconsin (LEF) and West Branch, Iowa (WBI) from NOAA's Global Greenhouse Gas Reference Network)²⁸ to examine the imprint of crop production on the regional CO₂ seasonal cycle. Through a statistical examination of these long-term CO₂ records, together with inversion products of net ecosystem exchange (NEE; CarbonTracker 2019)²⁹, we quantified the sensitivity of net CO₂ exchange to interannual temperature variations and attribute this sensitivity to CO₂ exchange dynamics of croplands and natural ecosystems, respectively. The quantified sensitivity was then used to evaluate how the CO₂ seasonal cycle and net CO₂ uptake in the Corn Belt will respond to future climate warming by year 2050.

Results and discussion

Agricultural imprint on the CO₂ seasonal cycle. The decadal CO₂ records measured at KCMP, LEF, and WBI were de-spiked, gap-filled, and digitally filtered to extract the long-term CO₂ growth rate and the detrended CO₂ seasonal cycle (Fig. S1) (see Methods). To probe the link between the CO₂ seasonal cycle characteristics and crop production within the region, we defined a cropland fraction (f_{CS}), calculated as the ratio of land area of corn and soybean to total area of land ecosystems (i.e., croplands plus natural ecosystems) (see Methods). Over 2008 to 2018, f_{CS} was 0.43 ± 0.01 (1 σ), 0.12 ± 0.01 , 0.56 ± 0.01 within the intense concentration footprints (i.e., 300 km radius to each tower; see Methods) of KCMP, LEF, and WBI, respectively (Figs. S2 and S3), forming a unique gradient for examining the regional impact of corn and soybean on the CO₂ seasonal cycle. In addition, we take advantage of the heterogeneous land use within the intense concentration footprint of KCMP (Fig. S2) by sampling the hourly CO₂ concentrations based on wind direction. Two monthly CO₂ datasets were built using the northwesterly CO₂ observations (i.e., 270°–360°; hereafter, KCMP^{NW}) and the southern and south-eastern sector observations (i.e., 120°–210°; hereafter, KCMP^{SSE}) along the dominant wind directions (Fig. 1; see Methods). Notably, the south and southeast sector had a significantly higher f_{CS} (0.52 ± 0.01) compared to the northwest sector (0.23 ± 0.01).

The long-term growth rate of CO₂ (2.12 – 2.37 ppm yr⁻¹) was similar across the three tall tower sites and between the three sites and a continental background site without significant agricultural influences (2.26 ppm yr⁻¹; Niwot Ridge, Colorado; see Methods) (Fig. S1). The detrended CO₂ seasonal cycle at all three sites reached annual minimum values in late July/early August after a period of rapid CO₂ drawdown and then increased gradually until December (Fig. 2b). Compared to NWR, all three sites had earlier and larger CO₂ drawdowns and more elevated CO₂ concentrations during the dormant season (October–April next year) (Fig. 2b), indicating vigorous C source and sink activities within this highly productive region. Among the three tower sites, WBI had the largest average annual CO₂ drawdown (-19 ppm), followed by KCMP (-18 ppm), and LEF (-15 ppm) (Fig. 2e). Correspondingly, the average CO₂ seasonal amplitude was largest

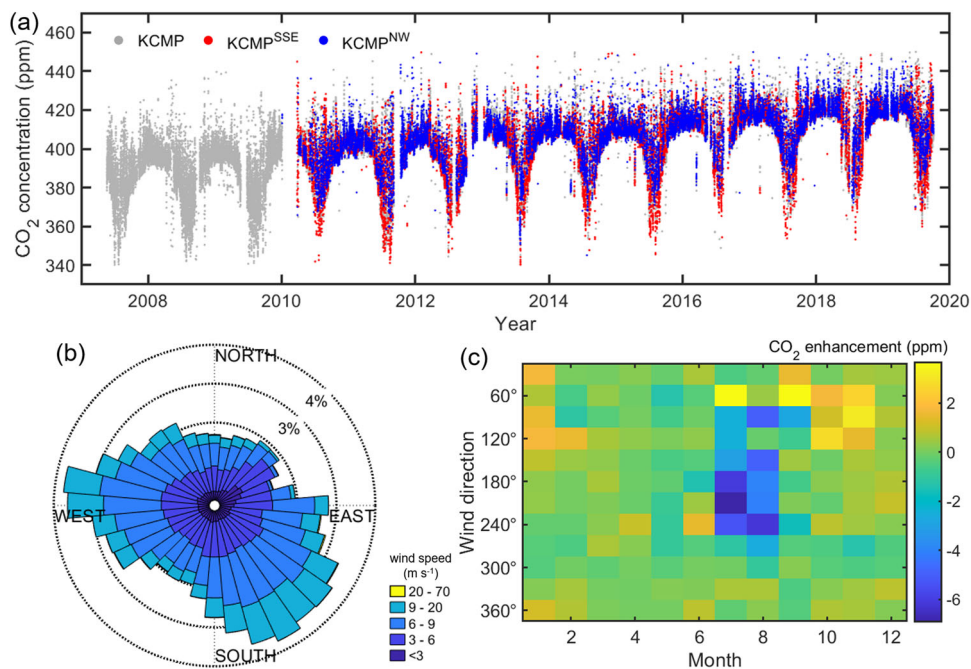


Fig. 1 CO₂ concentration measured at KCMP. **a** Hourly CO₂ concentration measurements made from 2008 to 2018. **b** Wind rose showing distributions of wind direction and speed during 2010 to 2018. **c** Enhancement of CO₂ concentration relative to the northwestern sector (270°–360°) when wind speed was greater than 3 m s⁻¹.

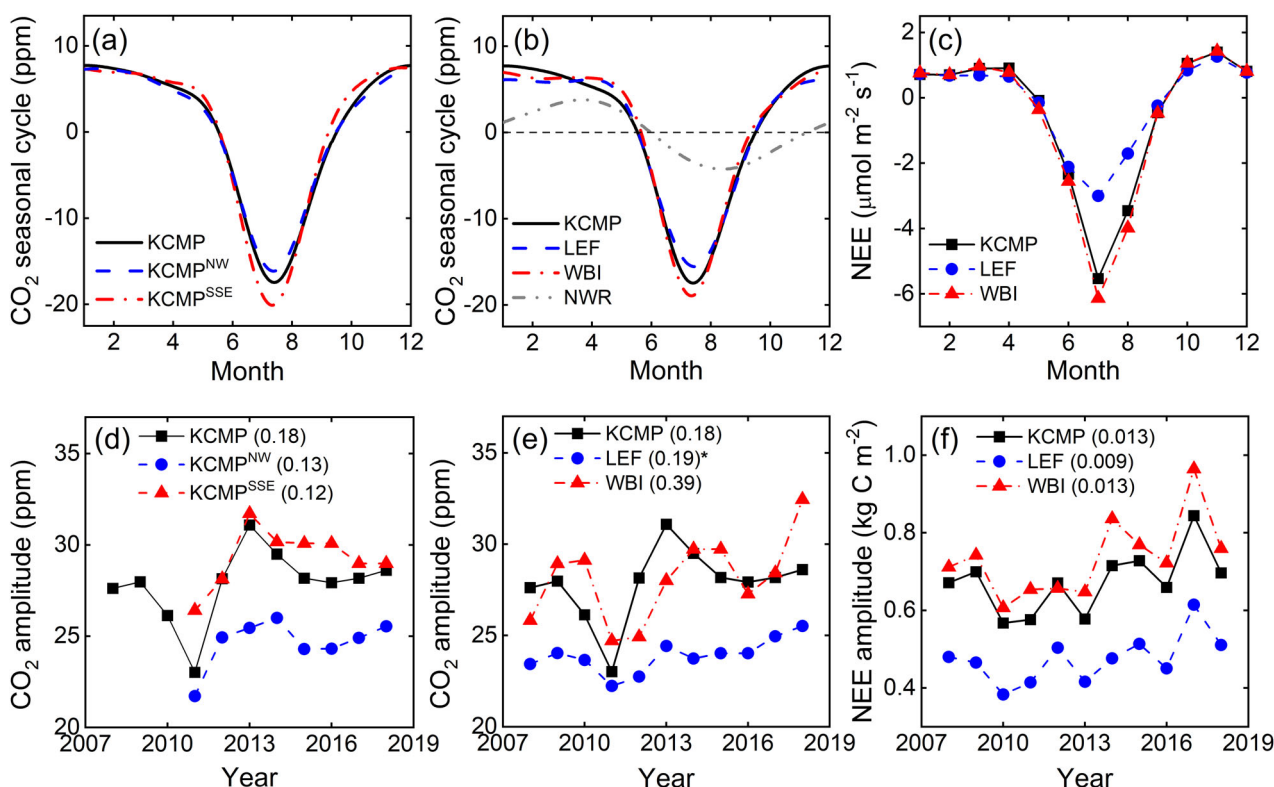


Fig. 2 The annual CO₂ exchange metrics at the three tall tower sites. The detrended CO₂ seasonal cycle (**a**, **b**) and the CarbonTracker NEE (**c**) averaged over the entire observation period. The CO₂ seasonal amplitude (**d**, **e**) and the NEE amplitude **f** at the three tall tower sites. Trends in the annual CO₂ exchange metrics were estimated using the nonparametric Theil–Sen estimator and shown in the legend. Statistically significant trends (the Mann–Kendall trend test; $P < 0.1$) are indicated by an asterisk symbol in the legend.

at WBI (28.1 ppm), followed by KCMP (27.9 ppm) and LEF (23.9 ppm) (Fig. 2e). These spatial gradients are in concordance with the large differences in f_{CS} and the growing season (May–September) NEE among the three sites (Fig. 2c). The strong sensitivity of the CO₂ seasonal cycle to corn and soybean production is also highlighted by the larger CO₂ drawdown and seasonal amplitude of KCMP^{SSE} compared to KCMP^{NW} (Fig. 2a, d). To further examine the convolution between atmospheric transport, land use, and the CO₂ seasonal cycle, we subtracted the northwestern sector (270°–360°) measurements binned by month from the monthly mean of the CO₂ concentration in 12 evenly spaced directional sectors around KCMP. From this wind sector analysis, a clear depletion of CO₂ is evident in the peak growing season (i.e., July and August) when winds were coming from the heart of the Corn Belt (i.e., south and southeast) (Fig. 1c). Collectively, these results underscore a large spatial gradient in the atmospheric CO₂ concentrations within the study domain and corroborate the strong imprint of crops on regional CO₂ uptake^{26,30}.

Over the 11-year analysis, total production and yields of corn and soybean increased significantly (the Mann-Kendall test; $P < 0.1$) within the intense concentration footprints of KCMP and WBI (Fig. S5). The increasing yield trends are consistent with the continued growth in crop productivity over the entire Corn Belt and can be attributed to several possible mechanisms related to advances in breeding and genetic technology (e.g., longer maturity cultivars that can adapt to higher sowing density), agronomic practices (e.g., improved herbicide and weed management), and favorable growing conditions (e.g., enhanced water use efficiency under rising atmospheric CO₂)³¹. Over the study period, the CO₂ seasonal amplitude increased at a rate of 0.18 ppm yr⁻¹ (the nonparametric Theil–Sen estimator) and 0.39 ppm yr⁻¹ at KCMP and WBI, respectively (Fig. 2c), although the trends are not statistically significant (the Mann-Kendall test; $P = 0.12$ for KCMP and $P = 0.14$ for WBI). In contrast, the CO₂ seasonal amplitude observed at LEF exhibited much smaller interannual variability than those at KCMP and WBI (Fig. 2e), and a significant increasing trend of the CO₂ seasonal amplitude (0.19 ppm yr⁻¹; $P < 0.1$) was evident (Fig. 2e). To compare with the seasonal amplitude of CO₂, we have also calculated the annual amplitude of NEE using the NEE inversion products within the intense concentration footprints of the three tall tower sites (see Methods). While the mean magnitude of the annual NEE amplitude varied across the three sites, consistent with the CO₂ seasonal amplitude, significant trend was absent at any site (Fig. 2f). To further examine causal relationships between crop yields and the CO₂ exchange dynamics, a correlation analysis (Pearson correlation coefficient) was applied after a linear detrending of all the variables. No significant correlation ($P > 0.1$) was detected between crop yield anomalies and the CO₂ concentration- or NEE-based annual metrics at any of the three sites.

Therefore, although the agriculture intensification at northern mid-latitudes is believed to be an important driver of the increasing CO₂ seasonal amplitude in the northern hemisphere across the decadal to multi-decadal scales^{23,24}, our results, based on direct observations over an intensively agricultural region, suggest a decoupling between crop yields and CO₂ exchange intensity at the interannual scale. Because the CO₂ seasonal amplitude is an integrated measure of annual CO₂ exchange, this decoupling may be due to compensating responses of photosynthesis and ecosystem respiration to variations in climatic forcings at sub-annual scales⁵. Moreover, the large differences in magnitude and seasonal dynamics between KCMP^{NW} and KCMP^{SSE} (Fig. 1) imply that changes in atmospheric transport and circulation may have also played a role in weakening the interannual association between crop yields and atmospheric

CO₂^{11,16}. On the other hand, although grain yield constitutes a large fraction of crop NPP, the extent to which assimilated C in crops is partitioned to grain depends on whether and when the temperature threshold has been exceeded^{31,32}, implying an intricate climate modulation on the yield–CO₂ relationship. Notably, the past decade exhibited numerous extreme temperature and precipitation variations in the U.S. Midwest. The long-lasting and pervasive heat wave and drought in the spring and summer of 2012 damaged a substantial proportion of crop commodities³³ and adversely affected the functionality of natural ecosystems in this region³⁴; notwithstanding, four of the wettest years in the last 100 years (ranks 1–4) were also recorded in the past decade³⁵. These large interannual climate variations provide a natural experiment to observe the behavior of terrestrial ecosystems under anomalous climate conditions, making it possible to unravel the dynamic link among climate, crop production, and CO₂ exchange at scales finer than the annual scale.

Temperature sensitivity of the CO₂ exchange anomalies. To examine how changes in the CO₂ seasonal cycle were linked to temperature variations at the monthly scale, we calculated the first-time derivative of the CO₂ time series, ΔCO_2 (Fig. S6), which has been demonstrated to be a better proxy of net land-atmosphere CO₂ fluxes than the original CO₂ seasonal cycle at northern latitudes³⁶. The sensitivity of ΔCO_2 (or NEE) anomaly to temperature variations (β_T) within the intense concentration footprint of each tall tower site was then estimated as the slope of the regression on temperature in a multiple linear regression (MLR) of ΔCO_2 (or NEE) against temperature, water availability (i.e., 3-month cumulative precipitation including the current month; see Methods), and radiation (all variables detrended). Climate variations explained 14–65% and 19–81% of variances in the ΔCO_2 and NEE anomalies of individual months, respectively (Fig. S7 and S8). The climate anomalies explained a much larger fraction (i.e., >60%) of ΔCO_2 and NEE variances in the growing season months than in the dormant season (Figs. S7 and S8), signifying the important role of climate–vegetation interactions in controlling the regional CO₂ exchange variability.

There were pronounced seasonal patterns in β_T of ΔCO_2 and NEE at all three tall tower sites (Fig. 3; Supplementary Data 1 and 2). Notably, β_T of both ΔCO_2 and NEE were significantly positive (i.e., an increase in monthly mean temperature leads to reduced net CO₂ uptake) in July and August, whereas only β_T of NEE was significantly negative in June at KCMP and WBI (Fig. 3). A correlation analysis (Pearson correlation coefficient) between the monthly ΔCO_2 and NEE anomalies shows that the ΔCO_2 and NEE anomalies were significantly ($P < 0.05$) and positively correlated in summer (July and August) and early spring (April and/or May) at all three sites, whereas no significant correlation emerged in June at any of the sites (Fig. S9). Because the NEE inversion products were derived taking into account atmospheric transport and circulation, the absence of significant correlation between ΔCO_2 and NEE in June suggests an important role of air mass transport and mixing in determining the temperature– ΔCO_2 relationship at the regional scale³⁷. Despite large interannual variations in dormant season air temperature (data not shown), β_T of ΔCO_2 and NEE were mostly small and not significantly different from zero in the dormant season months (Fig. 3). It is noteworthy that incorporating uncertainties in defining the concentration footprints did not qualitatively change the estimated β_T of ΔCO_2 and NEE at any of the three tall tower sites (see Methods; Figs. S10 and S11).

A panel data model that combines the climate and NEE anomalies of the three tall tower sites was used to derive β_T of NEE specific to croplands (i.e., corn and soybean) and natural

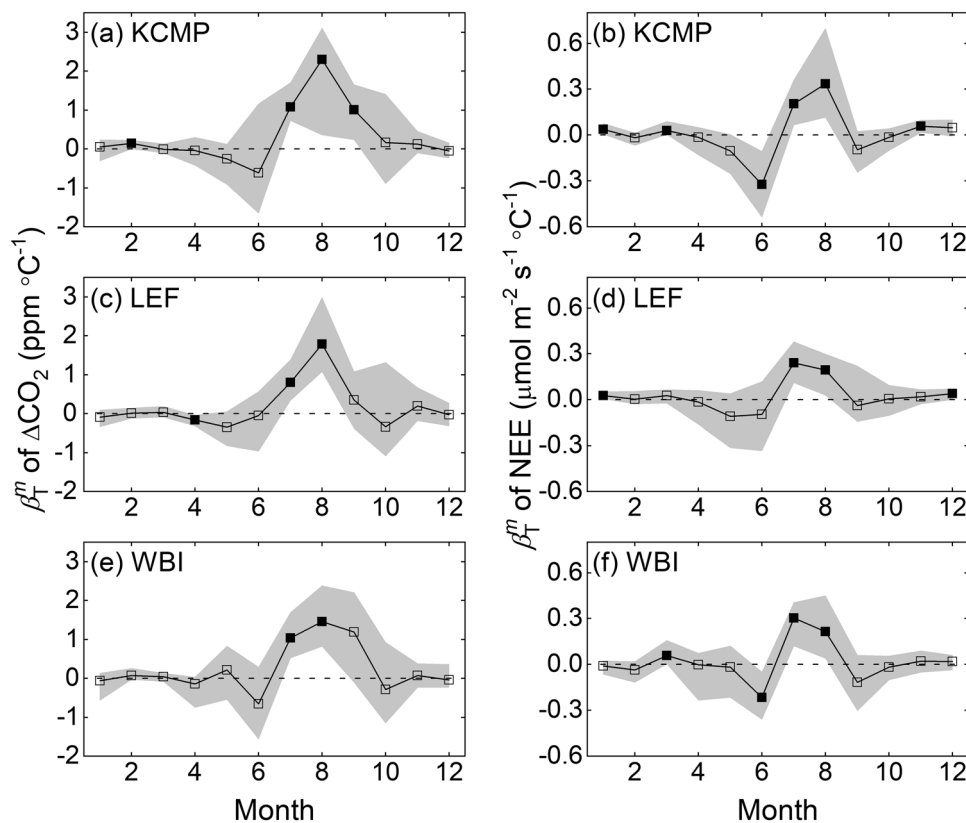


Fig. 3 Temperature sensitivity of ΔCO_2 and NEE within the intense concentration footprints (300 km radius) of KCMP, LEF, and WBI. Panels **a** and **b**, **c** and **d**, and **e** and **f** are for KCMP, LEF, and WBI, respectively. Gray shaded area denotes the 90% confidence interval of estimated sensitivity derived through resampling. Sensitivities significant at the 90% confidence level are denoted by solid squares.

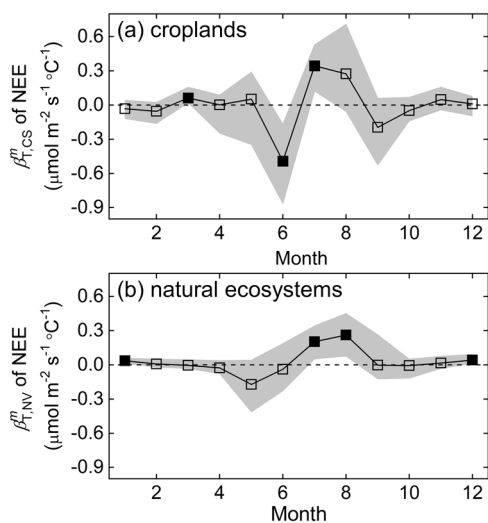


Fig. 4 Biome-specific temperature sensitivity of NEE for croplands and natural ecosystems. Panels **a** and **b** are for croplands and natural ecosystems, respectively. Gray shaded area denotes the 90% confidence interval of estimated sensitivity derived through resampling. Sensitivities significant at the 90% confidence level are denoted by solid squares.

terrestrial ecosystems (see Methods). This approach leverages the contrasting f_{CS} across the three sites and assumes that the differences in climate sensitivities between croplands and natural ecosystems were coherent within the domain of the three tower sites (see Supplementary Discussion for an extended discussion). The estimated biome-specific β_T can therefore be viewed as an area- and CO_2 flux-weighted net temperature sensitivity that

encompasses the entire range of ecosystem processes by which temperature impacts ecosystem CO_2 exchange within each biome category. The estimated biome-specific β_T illuminates the dominant role of croplands in driving the negative β_T of NEE in June, while NEE of both croplands and natural ecosystems responded positively to temperature variations in July and August (Fig. 4; Table S1). These results are robust for a range of tower footprint radii (150–450 km) used in the panel analysis (Fig. S13) and are not sensitive to changes in the definition of the two biome categories (Fig. S14).

The negative temperature impact on cropland NEE in June (i.e., higher temperature favors enhanced CO_2 uptake) is consistent with the rapid phenological development of corn and soybean during this critical transition period when cumulative thermal energy typically meets the threshold of crop leaf emergence in the Corn Belt (Fig. S15a)³⁸. Field evidence shows that during this early vegetative stage, the positive feedback between crop canopy development and photosynthetic capacity amplifies the response of crop photosynthesis to temperature variations, leading to accelerated crop growth under warmer temperatures^{32,39}. Furthermore, the negative β_T in June might have been an indirect result of human responses to spring climate variations⁴⁰. In the Corn Belt, the timing of crop planting is largely determined by temperature and precipitation in early spring⁴¹. Earlier crop planting in years with warm and dry springs can therefore hasten crop growth in early to mid-spring, giving rise to a stronger photosynthetic response to temperature in late spring to early summer. Indeed, there was a significant linear relationship between the anomaly of June NEE and anomaly of simulated corn leaf emergence date (CLED) within the intense concentration footprints of KCMP and WBI (Fig. S15b; see Methods). This positive correlation remains robust at both sites after removing the control of June temperature

variations (Partial correlation analysis; $P < 0.1$), underpinning a crop phenology-mediated legacy effect of early spring temperature variations on CO_2 uptake in June. On the other hand, in contrast to previous studies in temperate deciduous and evergreen forests^{17,18}, natural ecosystems within the study domain did not show a strong response to temperature variations during spring to early summer (Fig. 4b). Importantly, with the tower footprints on the order of several hundreds of kilometers (Fig. S4), the derived β_T inherently represents a net sensitivity across a diversity of ecosystem types (e.g., grasslands, forests, and wetlands). As a result, the lack of coherent temperature response likely reflects asynchronous temperature–phenology regimes among different natural ecosystems that compensates temperature-driven NEE anomalies with increasing levels of spatial aggregation^{42,43}.

While most previous long-term C cycle studies in northern ecosystems have concentrated on the temperature–phenology– CO_2 interactions in spring and autumn^{12,18}, less attention has been given to the interannual relationship between temperature and CO_2 anomalies at the height of the growing season¹⁴. Our analyses, based on either ΔCO_2 or NEE anomalies, unequivocally identified positive β_T of net CO_2 exchange (i.e., higher temperature reduces net CO_2 uptake) in both croplands and natural ecosystems during the peak growing season (Figs. 3 and 4), where temperature is highest within a year and plants reach their peak photosynthetic capacity in this region^{38,42}. High temperatures affect NEE of crop and natural ecosystems through a variety of direct and indirect pathways. At the ecosystem scale, a well-accepted conceptual model is that photosynthesis responds to temperature variations following a quadratic function, defined by a maximum photosynthetic rate at optimal temperature⁴⁴, whereas ecosystem respiration increases with temperature through stimulated metabolic rates in an exponential fashion⁴⁵. Therefore, a positive summer β_T can be an indicator of ecosystems operating beyond their thermal optima of photosynthesis. In addition, high temperatures can also suppress photosynthesis and ecosystem productivity by imposing water stress on plants^{46,47}. High summer temperatures not only limit soil water supply by sustained evapotranspiration but also increase atmospheric water demand by increasing the vapor pressure deficit (VPD) of the atmosphere. In response to increased VPD coupled with limited soil moisture, plants close their stomata to prevent excessive water loss, at the cost of reduced CO_2 uptake^{48,49}. Importantly, this temperature-induced negative impact on plant CO_2 uptake is exacerbated by insufficient summer precipitation, resulting in heat and drought stresses on ecosystem productivity⁵⁰.

To gain insight into the importance of this potential interaction between temperature and water availability (i.e., 3-month cumulative precipitation including the current month) in driving the summer CO_2 exchange anomalies, we estimated the summer temperature sensitivity under different water availability conditions. Specifically, we transformed the climate variables and CO_2 exchange of July and August to z-score anomalies using their monthly means and standard deviations, pooled the z-score anomalies of the three tower sites, and grouped this combined dataset into four bins: dry (z-score less than -1), moderate dry (z-score between -1 and 0), moderate wet (z-score between 0 and 1), and wet (z-score greater than 1) summers. An MLR was then applied to estimate β_T for each bin. As shown in Fig. 5, β_T of ΔCO_2 and NEE were significantly greater in dry summers than in other bins of summer water availability, indicating that dry conditions indeed increased summer β_T by imposing plant water stress that can also lead to lowered temperature optimum for photosynthesis^{44,50}. However, even in summers with above average water availability (i.e., moderate wet and wet summers), β_T of ΔCO_2 and NEE were significantly positive (Fig. 5), suggesting that both croplands and natural ecosystems have adapted to current summer temperature and were operating at their thermal optima of CO_2

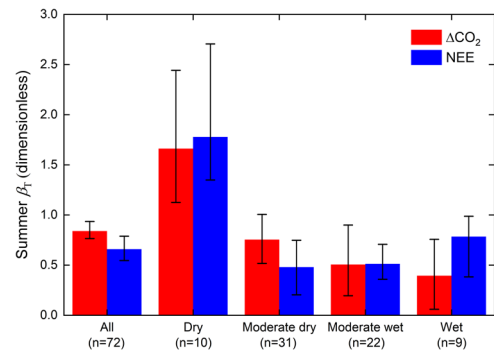


Fig. 5 Temperature sensitivity of ΔCO_2 and NEE for different bins of summer water availability. Error bar denotes the 90% confidence interval of estimated sensitivity derived through resampling (i.e., deemed significant at the 90% confidence level if the error bar does not contain zero). Sample size for each bin is also shown.

uptake. Thus, high summer temperatures caused reduced net CO_2 uptake in this mesic, seasonally cold region both during drought and modestly dry periods that regularly occur in the peak growing season⁵¹.

The finding that the summer CO_2 uptake of croplands has already reached its thermal optimum implies a strong temperature control on crop production in the Corn Belt. In light of the revealed β_T of ΔCO_2 and NEE, we used a panel data model with mean spring temperature (i.e., May and June), summer temperature (i.e., July and August), and growing season precipitation as the explanatory variables to probe the linkage between climate and crop yield variations within the footprints of KCMP and WBI (see Methods). The model results show that temperature and precipitation variations together with an increasing yield trend explain about 80% of variances in corn yields at the two sites (Fig. S16a, S16b; Table S2) and that higher summer temperature reduced corn yield at a rate of $-0.36 \text{ t ha}^{-1} \text{ }^\circ\text{C}^{-1}$ (90% CI: -0.54 to $-0.19 \text{ t ha}^{-1} \text{ }^\circ\text{C}^{-1}$ with a base summer temperature of 23°C), or about $3.0\% \text{ }^\circ\text{C}^{-1}$, in strong agreement with previous findings (e.g., 2.5% reduction for every 0.8° rise above 23°)⁵². Evidence from agronomic research shows that July and August correspond to the critical reproductive stage of corn (i.e., grain filling) in the Corn Belt and that temperature stress during this stage of corn growth contributes directly to yield reduction by shortening the grain filling period and reducing the translocation of photosynthate into reproductive biomass (i.e., lower harvest index)³¹. On the other hand, although higher spring temperature has favored net CO_2 uptake (Fig. 4a) and thus vegetative development of corn, the effect of spring temperature on the final corn yield was not significant (Table S2). This finding is in line with results from recent heating experiments conducted in the central Corn Belt that warmer leaf temperatures during the vegetative stage do not exert lasting effects on corn reproductive growth, possibly due to the high optimal temperature of photosynthesis relative to the background spring temperature during this period^{32,53}.

Interestingly, while growing season precipitation had a significant positive impact on soybean yields within the footprints of KCMP and WBI, neither spring nor summer temperature was significantly correlated with soybean yield variations over the 11-year analysis (Fig. S16c, S16d; Table S3). The lack of significant temperature effect on soybean yields has been previously reported by Lobell et al.⁴⁶ using historical (1995–2012) soybean yield records in the central Corn Belt. Given that atmospheric CO_2 concentrations increased by ~ 30 ppm over the 11-year span at KCMP and WBI, temperature effects of soybean yields may have been confounded by the

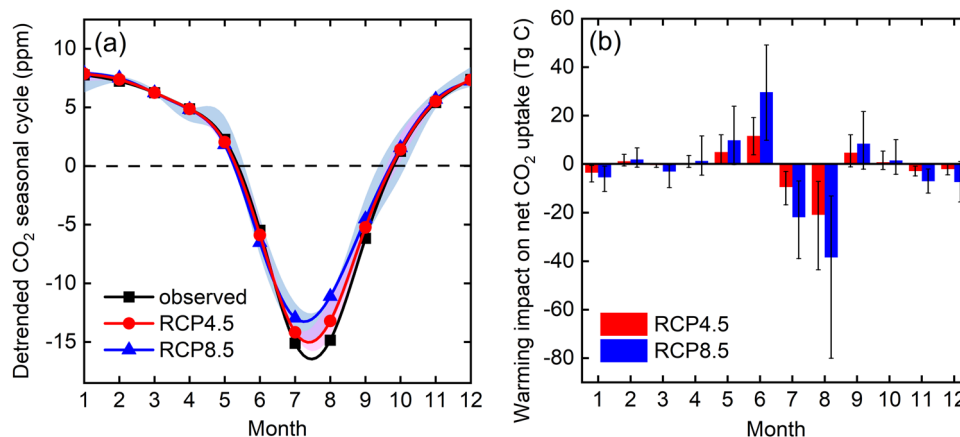


Fig. 6 Changes in the detrended CO₂ seasonal cycle and net CO₂ uptake in the Corn Belt under future warming scenarios by 2050. Black squares and line in **a** denote the observed average seasonal cycle of CO₂ during 2008–2018. Shaded area in **a** and error bars in **b** denote 90% confidence intervals derived through resampling. It is important to note that in **b**, a negative warming impact denotes reduced net CO₂ uptake under the future warming scenarios.

CO₂ fertilization effect, which has been shown to alleviate temperature stress on soybean reproductive development by enhancing soybean water-use efficiency and photosynthesis⁵⁴, but have no significant impact on corn yields⁵³. These results imply a dominant control of corn in mediating the link between temperature variations and cropland CO₂ exchange within the study domain. Indeed, there was a significantly negative relationship between the detrended corn yield anomaly and the anomaly of July NEE within the intense footprints of KCMP and WBI (ordinary linear regression; $P < 0.05$) (Fig. S17). This direct connection between corn yield and July NEE was persistent even without including 2012 – a historical bad year for corn yields in this region (Fig. S17). Therefore, despite the decoupling between crop yields and CO₂ exchange intensity at the annual scale, this study highlights a dynamic modulation of temperature on cropland CO₂ exchange and crop yields, which provides important implications for the impact and adaptation of crop production systems to future climate warming.

Implications for carbon cycle impacts of future climate warming. Projected climate data were retrieved from 10 general circulation models that have contributed to the Coupled Model Intercomparison Project Phase 5 (CMIP5) and run under the RCP4.5 and RCP8.5 scenarios (see Methods). Ensemble mean projections of average air temperature change by 2050 in the Corn Belt were roughly 2 °C for most months under RCP8.5 and between 0 °C and 2 °C under RCP4.5 (Fig. S18a). In contrast to the unanimous warming, models were mixed in the direction of projected precipitation and radiation changes under both the RCP4.5 and RCP8.5 scenarios, resulting in small overall monthly changes (e.g., $\pm 10\%$) relative to inter-model variability in both cases (Fig. S18b, S18c). Because the land use characteristics (Fig. S3), crop yields (Fig. S5), and CO₂ exchange dynamics (Fig. S19) of KCMP are representative of the broader Corn Belt (see Supplementary Discussion for an extended discussion), we applied the projected mean temperature changes to the estimated β_T of KCMP and its uncertainty to predict how future climate warming may impact the CO₂ seasonal cycle and net CO₂ uptake in the Corn Belt. Here, we define the Corn Belt by those states in the U.S. Midwest with significant corn and soybean land use (Fig. S19)^{55,56}. The total area of land ecosystems within the Corn Belt is estimated at 148 million ha⁵⁵. It is important to note that all the projected mean air temperature changes in the Corn Belt

are within the range of historical observations at KCMP (2010–2019; Fig. S18a), which improve the plausibility of extrapolating to future warming scenarios.

Assuming a stasis of seasonal changes in atmospheric transport and circulation, warming in the next decades could alter the trajectory of the CO₂ seasonal cycle (Fig. 6a). Higher summer temperature will limit CO₂ drawdowns and consequently attenuate the CO₂ seasonal amplitude from the current level by 1.5 ppm (~5%) to 3 ppm (~10%) under the two warming scenarios (Fig. 6a). This prediction is in line with the emerging negative impact of warming on summer CO₂ drawdown in boreal ecosystems ($-2.06 \text{ ppm } ^\circ\text{C}^{-1}$)¹⁴ and suggests that the loss of stimulating effects of warming on the CO₂ seasonal amplitude, as recently discovered at the northern high latitudes ($>50^\circ\text{N}$)¹³, may have a larger spatial extent than previously thought. Extrapolating to the land ecosystems of the entire Corn Belt, the negative warming impact can reduce net CO₂ uptake during the peak growing season by 30 Tg °C (90% CI: 10 to 60 Tg °C) under RCP4.5 and 60 Tg °C (90% CI: 20 to 117 Tg °C) under RCP8.5, equivalent to approximately 10 to 20% of the annual net CO₂ sequestration (i.e., 292 Tg °C; Fig. S19) of this highly productive region (Fig. 6b). This negative warming impact, however, can be partially offset by the positive impact in June (12 to 29 Tg °C under the two warming scenarios) and, to a lesser extent, May (5 to 10 Tg °C) (Fig. 6b), as a result of crop phenological development. Integrated over the entire growing season, warming by 2050 is projected to reduce the net CO₂ uptake by 9 Tg °C (90% CI: reduction by 54 to enhancement by 36 Tg °C) to 13 Tg °C (90% CI: reduction by 92 to enhancement by 55 Tg °C) under the two warming scenarios, although this negative impact is not significant at the 90% confidence level under either scenario due to the compensatory temperature effects on spring and summer CO₂ uptake. Combining phenology observations with ecosystem-scale NEE measurements, Keenan et al.¹⁸ showed that increased spring and fall temperature has lengthened the growing season of temperate forests over the eastern U.S. (total land area = 38 million ha), leading to enhanced CO₂ uptake at a rate of 16 g C m⁻² per 1 °C increase in spring or fall. Applying this increasing rate of CO₂ uptake to the future warming scenarios suggests an annual gain of CO₂ sequestration ranging from 9 to 23 Tg °C in these systems. While it is unclear how these systems are currently responding to temperature variations in summer, this projected increase in net CO₂ uptake is of similar magnitude to the net reduction of growing season CO₂ uptake in the Corn Belt. Collectively, these results highlight that overall magnitude and timing of future climate

warming could be equally critical in determining the C sink strength of terrestrial ecosystems at northern temperate latitudes.

It is important to note that the projected warming impacts, based on the average monthly temperatures, do not account for substantial reduction in CO₂ sink strength by extreme heat events^{34,46}, which are expected to continue increasing in frequency and severity in the future⁵⁷. Besides the direct and indirect physiological impacts of warming discussed above, the regional CO₂ seasonal cycle and CO₂ sink strength are also modulated by a myriad of slow-evolving and climate-sensitive processes (e.g., CO₂ fertilization effect, soil C turnover, and nutrient cycling)⁵⁸, which may not vary linearly with the projected future warming at multi-decadal scales. Furthermore, the projected future warming impacts can be countered by adaptation measures taken by farmers, such as changes in planting dates or use of longer-maturing cultivars⁴⁰. For example, earlier planting may be enabled by warmer spring temperatures in the future. Shifts in development timing will therefore modulate the weather experienced by crops and may alleviate the adverse effects of higher summer temperatures. Because our projection does not account for farmer adaptations, the projected warming impacts on the CO₂ uptake can be viewed as the expectation in the absence of explicit recognition of, and adaptation to, temperature trends from present to 2050. Thus, a key question that remains to be answered is whether the revealed negative warming impacts on net CO₂ uptake in northern terrestrial ecosystems indicate a future climatic tipping point for CO₂ sequestration and plant productivity in these dynamical systems. Regardless, this study challenges the paradigm that warming will continue to benefit CO₂ sequestration in terrestrial ecosystems at northern mid-latitudes and emphasizes the need to robustly represent the temperature sensitivity of cropland CO₂ exchange for current climate in C cycle models in order to improve the predictability of future carbon-climate feedbacks.

Methods

Atmospheric CO₂ concentration. The tall tower CO₂ observations reported here were measured from April 2007 to December 2019 at the University of Minnesota tall tower Trace Gas Observatory (KCMP tall tower; 44.6888°N, 93.0728°W) (Fig. S2a). Air was pulled continuously from 100 m above ground to the base of the tower, where it was dried, subsampled, and measured for CO₂ concentration at 10 Hz using a tunable diode laser spectrometer (TGA100A, Campbell Scientific Inc., Logan, Utah, USA). The calibrated 10 Hz data were then block averaged into hourly values, with a long-term precision of 0.2 ppm. Wind speed and direction at 100 m were measured using a sonic anemometer (CSAT3, Campbell Scientific, Logan, Utah, USA). Further details regarding the tall tower sampling and calibration scheme can be found in Griffis et al.⁵⁹. CO₂ concentration data collected from 2007 to 2010 have already been reported by Zhang et al.²⁷ and Hu et al.³⁷ in assessments of regional-scale CO₂ fluxes. Here we use all available data and focus our analyses on the CO₂ seasonal cycle at the interannual timescale.

Two additional long-term tall tower sites from NOAA's Global Greenhouse Gas Reference Network, Park Falls, Wisconsin (LEF; 45.9451°N, 90.2732°W) and West Branch, Iowa (WBI; 41.7248°N, 91.3529°W), are located within the region and were used in this study (Fig. S2a). Hourly CO₂ concentration data measured at LEF and WBI from 2007 to 2018 at 99–122 m above ground were obtained from NOAA's ObsPack data products²⁸.

The hourly CO₂ time series of the three tall tower sites were de-spiked, gap-filled, and block averaged into daily values (see Supplementary Methods for more details). Following the method of Barlow et al.³⁶, a wavelet transform was used to spectrally decompose the daily CO₂ time series. The detrended seasonal cycle and long-term growth of CO₂ were then isolated by summing frequencies at periods of 3–18 months and >18 months, respectively³⁶ (Fig. S1; see Supplementary Methods for more details). The CO₂ seasonal amplitude was obtained as the peak-to-trough difference of the detrended seasonal cycle.

To examine how the CO₂ seasonal cycle measured at KCMP was mediated by the convection of atmospheric transport and ecosystem CO₂ exchange, we sampled the KCMP CO₂ time series based on wind direction for the period 2010–2018, where we have complete wind data at 100 m height. We only considered the hourly CO₂ data with wind speed greater than 3 m s⁻¹ to reduce local source effects^{60,61}. Two CO₂ datasets (KCMP^{NW} and KCMP^{SSE}) were built for the dominant wind directions 270°–360° (northwest) and 120°–210° (south and southeast), respectively (Fig. 1a, b). The CO₂ seasonal cycle characteristics of

KCMP^{NW} and KCMP^{SSE} were extracted using the same wavelet method described above.

To infer the CO₂ source and sink strength within the Corn Belt, we compared the CO₂ seasonal cycle measured at the three tower sites with continental background CO₂ measured at Niwot Ridge (NWR; 40.0531°N, 105.5864°W; managed by NOAA's Earth System Research Laboratory; Fig. S4). The NWR site sits approximately 27 km west of Boulder, Colorado, and 6 km east of the Continental Divide (Fig. S4). Although climate and biota of the site are characterized by alpine ecosystems, NWR, at an altitude of 3526 m (3523 m elevation; 3 m intake height), is well situated to measure CO₂ concentrations in well-mixed continental boundary layer that are representative of large areas without significant influences from local anthropogenic emissions^{62,63} and agricultural activities⁵⁵. Weekly CO₂ concentrations measured at NWR from 2007 to 2018 were obtained from NOAA's ObsPack data products²⁸.

Concentration footprint. Detailed footprint analyses have been conducted by Hu et al.³⁷ for KCMP using the Stochastic Time-Inverted Lagrangian Transport model⁶⁴. From these analyses, 80% of the concentration signal (i.e., sensitivity of concentration variations to surface CO₂ exchanges) originated from an area within 307, 255, 302, and 298 km radius of KCMP for the four seasons, respectively (Fig. S4)³⁷. Therefore, we define a 300 km radius as the intense concentration footprint for all three tall towers by assuming that the area within this intense footprint has equally weighted influence on the CO₂ observations. We also test a range of radii (150–450 km) to gauge how the definition of intense concentration footprint impacts our analyses and conclusions.

Net ecosystem exchange from atmospheric inversions. Monthly terrestrial biosphere net ecosystem CO₂ exchange (NEE) within the tower footprints were obtained from the CarbonTracker assimilation system for 2007–2018 (CT2019)²⁹. The CarbonTracker NEE is an inverse product (1° × 1°) derived from a priori NEE estimates from terrestrial biosphere models and optimized using simulated atmospheric transport and in situ atmospheric CO₂ measurements (including LEF and WBI). Zhang et al.²⁷ compared the CarbonTracker NEE to eddy covariance-based bottom-up estimates of NEE within a radius of 200–600 km to KCMP and found excellent agreement between the two methods (Nash–Sutcliffe efficiency (NSE) > 0.9), indicating that the CarbonTracker NEE is sensitive to the heterogeneous C exchange activities within the study domain. Using the NEE data within the intense concentration footprints of the three tower sites, we calculated the annual amplitude of NEE, defined as the difference in cumulative NEE between the dormant season (October–April next year) and the growing season (May–September).

Land use characteristics. High resolution (30 m) land cover data were obtained from the USDA's National Agricultural Statistical Service National Cropland Data Layer (NCDL) for 2008–2018. We define an index, f_{CS} , calculated as the ratio of land area of corn and soybean to total area of land ecosystems (i.e., croplands plus natural ecosystems), to quantify the fractional influence of corn and soybean within each tower concentration footprint (Fig. S3). Pasture, spring and winter wheat, oats, and perennial crops such as alfalfa hay, which were present to various degrees within the concentration footprints of the three tall tower sites (Fig. S2), were grouped into the category of natural ecosystems in this study because of the challenge of separating pastures from natural grasslands, as well as the long growing seasons of these crops relative to corn and soybean²⁶. More description of the land use characteristics is provided in Supplementary Methods.

Crop data. County-level corn and soybean statistics from 2008 to 2018 were retrieved from the USDA's Quick Stats 2.0 database. Total grain production and harvested area for counties that fall within or intercept the intense concentration footprints (300 km radius) of KCMP and WBI were aggregated to calculate annual crop yields (in the unit of t ha⁻¹) for the two sites.

Climate data. Gridded daily average air temperature (2 m), precipitation, and incoming shortwave radiation within the tower concentration footprints were obtained from the National Center for Environmental Prediction North American Regional Reanalysis (NCEP-NARR) for 2007–2019. Daily minimum and maximum air temperature data were obtained from PRISM climate data (<https://prism.oregonstate.edu/>). Projected climate data for 2006–2050 over the entire study domain were retrieved from 10 general circulation models that have contributed to the Coupled Model Intercomparison Project Phase 5 (CMIP5). We used projection data derived under two warming scenarios: RCP4.5 and RCP8.5. Importantly, RCP4.5 is a median scenario for future greenhouse gas emissions with modest climate mitigation, while RCP8.5 is a high emission scenario assuming no mitigation^{65,66}. Following the method of Lobell et al.⁶⁷, the projected climate data time series were downscaled to correct for biases in the coarse-scale outputs from the CMIP5 models. This downscaling ensures that the mean and variance of projected climate data match the observational record for the period 2008–2018, while preserving any simulated trends out to 2050. Changes by 2050 were then calculated as averages for 2041–2050 minus averages for 2010–2019.

Simulation of corn leaf emergence date. Corn leaf emergence date (CLEED) within the intense concentration footprints of KCMP and WBI was simulated using growing degree time (GDT) with a base temperature of 8 °C (Fig. S15a)³⁸. Corn leaf emergence occurs when GDT exceeds the threshold of 450 units, assuming that land managers have already planted their fields³⁸. Following the method of De Wit et al.⁶⁸, diel temperature cycles within the tower concentration footprints were approximated using daily minimum and maximum temperatures to enable accumulation of heat units on an hourly time step. Our previous research showed that CLED simulated using this method has close agreement with long-term observations made at multiple AmeriFlux sites throughout the Corn Belt (e.g., Minnesota, Iowa, Illinois, Nebraska)³⁸.

Statistical analyses. Monotonic trends in the annual CO₂ exchange metrics (i.e., the CO₂ seasonal amplitude and the NEE amplitude) and crop yields were tested using the Mann-Kendall trend test and then estimated using the nonparametric Theil-Sen estimator, which is a robust method and insensitive to outliers.

To examine how changes in the CO₂ seasonal cycle were linked to interannual temperature variations, the daily values of the detrended CO₂ seasonal cycle were block averaged into monthly values for calculation of the first time derivative of the CO₂ concentration (i.e., change in CO₂ concentrations from one month to the previous month), ΔCO₂ (Fig. S6). The monthly time series of ΔCO₂, NEE, and climate data were then linearly detrended (using the “detrend” function of MATLAB) for each month of the year to allow the following analyses to focus on the interannual relationship between temperature and CO₂ exchange anomalies (i.e., ΔCO₂ and NEE)⁶⁹. The interannual sensitivity of ΔCO₂ (or NEE) anomaly to temperature variations (β_T) for a given month was estimated as the slope of the regression of temperature in a multiple linear regression (MLR) of ΔCO₂ (or NEE) against temperature, water availability, and radiation, such that indirect effects arising from covariations between the climate anomalies are accounted for in deriving β_T (i.e., equivalent to a partial correlation between temperature and CO₂ exchange anomalies controlled for the effects of precipitation and radiation anomalies)⁵⁰. We constructed detrended time series of precipitation anomaly cumulated for various lag time durations (2–6 months) to account for potential legacy effects of precipitation on ecosystem CO₂ exchange⁷⁰ and found that using a 3-month cumulative precipitation (P_{3m}) anomaly in the MLR resulted in the best regression fits for the three tower sites in combination. Therefore, P_{3m} was used as an index of water availability for all subsequent analyses. Uncertainty in the estimated β_T due to finite historical observations was estimated using bootstrap resampling (1000 iterations).

To further contrast the temperature sensitivity between croplands (i.e., corn and soybeans) and natural ecosystems, we used a panel data model that combines the climate (ΔT, ΔP_{3m}, and ΔR) and NEE anomalies of each month, year, and site (superscripts m , y , and s) and decomposes the site-specific temperature, precipitation, and radiation sensitivities (i.e., β_T , $\beta_{P(3m)}$, and β_R) into sensitivities specific to croplands and natural ecosystems (subscripts CS and NV). This is achieved by weighting the climate sensitivities using the land fractions of croplands (i.e., f_{CS}) and natural ecosystems (f_{NV} ; $f_{NV} = 1 - f_{CS}$) within the tower footprints:

$$\Delta NEE^{m,y,s} = \left(f_{CS}^{y,s} \cdot \beta_{T,CS}^m + f_{NV}^{y,s} \cdot \beta_{T,NV}^m \right) \cdot \Delta T^{m,y,s} + \left(f_{CS}^{y,s} \cdot \beta_{P(3m),CS}^m + f_{NV}^{y,s} \cdot \beta_{P(3m),NV}^m \right) \cdot \Delta P_{3m}^{m,y,s} + \left(f_{CS}^{y,s} \cdot \beta_{R,CS}^m + f_{NV}^{y,s} \cdot \beta_{R,NV}^m \right) \cdot \Delta R^{m,y,s} + \epsilon^{m,y,s} \quad (1)$$

where $\epsilon^{m,y,s}$ stands for the error term for site s in month m and year y . The model performance was evaluated using R^2 for individual months. Confidence intervals of the biome-specific climate sensitivities were estimated using bootstrap resampling, assuming 10% uniform random error in f_{CS} . The key assumption underlying Eq. 1 is that although f_{CS} differed significantly, the biome-specific climate sensitivities were similar across the three tower sites. This assumption was evaluated by comparing the sensitivities reconstructed from the derived biome-specific sensitivities to the “true” sensitivities independently estimated from the MLR of each tower site. The results show that the site-specific climate sensitivities of NEE can be successfully reproduced by the biome-specific sensitivities and f_{CS} at all three sites (NSE > 0.9; Fig. S12). This lends strong support for the use of the panel model that unifies the C exchange and climate anomalies across this heterogeneous region. Please see Supplementary Discussion for an extended discussion on the panel data analysis and its validation.

Following the method of Zhu et al.³¹, temperature sensitivity (γ) of corn yields (Y) within the intense concentration footprints of KCMP and WBI was estimated using a panel data model with mean spring temperature (i.e., May and June; T_{MJ}), summer temperature (i.e., July and August; T_{JA}), and growing season precipitation (P) as the explanatory variables:

$$Y^{y,s} = \gamma_1 \cdot t + \gamma_{MJ} \cdot T_{MJ}^{y,s} + \gamma_{JA} \cdot T_{JA}^{y,s} + \gamma_P \cdot P^{y,s} + C^s + \epsilon^{y,s} \quad (2)$$

where t denotes each year and $\gamma_1 \cdot t$ captures the yield increasing trend observed within the footprints of KCMP and WBI. C corresponds to fixed effects of each site and accounts for time-invariant site differences, e.g., the soil quality. $\epsilon^{y,s}$ stands for the error term for site s in year y . We did not include a quadratic term of temperature in the model because of the limited number of observations (22 site-years) and the fact that growing season temperature spanned a relatively narrow

range (e.g., 4.1° and 5.5° for mean July and August temperature at KCMP and WBI, respectively) during the study period.

Data availability

The hourly CO₂ concentration data measured at the KCMP tower from 2007 to 2019 have been deposited in the Environmental System Science Data Infrastructure for a Virtual Ecosystem (ESS-DIVE) (DOI: 10.15485/1634840) and are available for download at <https://data.ess-dive.lbl.gov/view/doi:10.15485/1634840>. Other data supporting the findings of this study are available in the supplementary information files.

Code availability

MATLAB codes for the statistical analyses are available upon request.

Received: 24 June 2020; Accepted: 7 January 2021;

Published online: 05 March 2021

References

- Climate change 2014: Synthesis report. Contribution of working groups I, II, and III to the Fifth Assessment Report of the Intergovernmental Panel on Climate Change (Core Writing Team, R. K. Pachauri & L. A. Meyer Eds). Geneva, Switzerland: IPCC, 151 pp.
- NOAA ESRL Global Monitoring Laboratory <https://www.esrl.noaa.gov/gmd/ccgg/> (2020).
- Le Quééré, C. et al. Global carbon budget. *Earth Syst. Sci. Data* **10**, 2141–2194 (2018).
- Shevliakova, E. et al. Historical warming reduced due to enhanced land carbon uptake. *Proc. Natl. Acad. Sci. USA* **110**, 16730–16735 (2013).
- Forkel, M. et al. Enhanced seasonal CO₂ exchange caused by amplified plant productivity in northern ecosystems. *Science* **351**, 696–699 (2016).
- Keeling, C. D., Chin, J. F. S. & Whorf, T. P. Increased activity of northern vegetation inferred from atmospheric CO₂ measurements. *Nature* **382**, 146–149 (1996).
- Graven, H. D. et al. Enhanced seasonal exchange of CO₂ by northern ecosystems since 1960. *Science* **341**, 1085–1089 (2013).
- Myneni, R. B., Keeling, C. D., Tucker, C. J., Asrar, G. & Nemani, R. R. Increased plant growth in the northern high latitudes from 1981 to 1991. *Nature* **386**, 698–702 (1997).
- Buermann, W. et al. Recent shift in Eurasian boreal forest greening response may be associated with warmer and drier summers. *Geophys. Res. Lett.* **41**, 1995–2002 (2014).
- Huang, K. et al. Enhanced peak growth of global vegetation and its key mechanisms. *Nat. Ecol. Evol.* **2**, 1897–1905 (2018).
- Wang, K. et al. Causes of slowing-down seasonal CO₂ amplitude at Mauna Loa. *Glob. Chang. Biol.* **26**, 4462–4477 (2020).
- Piao, S. et al. Weakening temperature control on the interannual variations of spring carbon uptake across northern lands. *Nat. Clim. Chang.* **7**, 359–363 (2017).
- Yin, Y. et al. Changes in the response of the Northern Hemisphere carbon uptake to temperature over the last three decades. *Geophys. Res. Lett.* **45**, 4371–4380 (2018).
- Wang, T. et al. Emerging negative impact of warming on summer carbon uptake in northern ecosystems. *Nat. Commun.* **9**, 1–7 (2018).
- Peñuelas, J. et al. Shifting from a fertilization-dominated to a warming-dominated period. *Nat. Ecol. Evol.* **1**, 1438–1445 (2017).
- Piao, S. et al. On the causes of trends in the seasonal amplitude of atmospheric CO₂. *Glob. Chang. Biol.* **24**, 608–616 (2018).
- Dragoni, D. et al. Evidence of increased net ecosystem productivity associated with a longer vegetated season in a deciduous forest in south-central Indiana, USA. *Glob. Chang. Biol.* **17**, 886–897 (2011).
- Keenan, T. F. et al. Net carbon uptake has increased through warming-induced changes in temperate forest phenology. *Nat. Clim. Chang.* **4**, 598–604 (2014).
- Foley, J. A. et al. Global consequences of land use. *Science* **309**, 570–574 (2005).
- Gilmanov, T. G. et al. Gross primary production and light response parameters of four Southern Plains ecosystems estimated using long-term CO₂-flux tower measurements. *Glob. Biogeochem. Cycles* **17**, 1071 (2003).
- Baker, J. M. & Griffis, T. J. Examining strategies to improve the carbon balance of corn/soybean agriculture using eddy covariance and mass balance techniques. *Agr. For. Meteorol.* **128**, 163–177 (2005).
- Guanter, L. et al. Global and time-resolved monitoring of crop photosynthesis with chlorophyll fluorescence. *Proc. Natl. Acad. Sci. USA* **111**, E1327–E1333 (2014).

23. Gray, J. M. et al. Direct human influence on atmospheric CO₂ seasonality from increased cropland productivity. *Nature* **515**, 398–401 (2014).
24. Zeng, N. et al. Agricultural green revolution as a driver of increasing atmospheric CO₂ seasonal amplitude. *Nature* **515**, 394–397 (2014).
25. Griffis, T. J. et al. Nitrous oxide emissions are enhanced in a warmer and wetter world. *Proc. Natl. Acad. Sci. USA* **114**, 12081–12085 (2017).
26. Miles, N. L. et al. Large amplitude spatial and temporal gradients in atmospheric boundary layer CO₂ mole fractions detected with a tower-based network in the US upper Midwest. *J. Geophys. Res.-Biogeophys.* **117**, G01019 (2012).
27. Zhang, X., Lee, X., Griffis, T. J., Baker, J. M. & Xiao, W. Estimating regional greenhouse gas fluxes: an uncertainty analysis of planetary boundary layer techniques and bottom-up inventories. *Atmos. Chem. Phys.* **14**, 10705–10719 (2014).
28. NOAA Earth System Research Laboratory, Global Monitoring Division, Multi-laboratory compilation of atmospheric carbon dioxide data for the period 1957–2018 (obspack_co2_1_GLOBALVIEWplus_v5.0_2019_08_12) <https://doi.org/10.25925/20190812> (2019).
29. Peters, W. et al. An atmospheric perspective on North American carbon dioxide exchange: CarbonTracker. *Proc. Natl. Acad. Sci. USA* **104**, 18925–18930 (2007).
30. Corbin, K. D. et al. Assessing the impact of crops on regional CO₂ fluxes and atmospheric concentrations. *Tellus B Chem. Phys. Meteorol.* **62**, 521–532 (2010).
31. Zhu, P., Zhuang, Q., Archontoulis, S. V., Bernacchi, C. & Müller, C. Dissecting the nonlinear response of maize yield to high temperature stress with model-data integration. *Glob. Chang. Biol.* **25**, 2470–2484 (2019).
32. Siebers, M. H. et al. Simulated heat waves during maize reproductive stages alter reproductive growth but have no lasting effect when applied during vegetative stages. *Agr. Ecosyst. Environ.* **240**, 162–170 (2017).
33. Mallya, G., Zhao, L., Song, X. C., Niyogi, D. & Govindaraju, R. S. 2012 Midwest drought in the United States. *J. Hydrol. Eng.* **18**, 737–745 (2013).
34. Wolf, S. et al. Warm spring reduced carbon cycle impact of the 2012 US summer drought. *Proc. Natl. Acad. Sci. USA* **113**, 5880–5885 (2016).
35. NOAA National Centers for environmental information (2020) climate at a glance. <https://www.ncdc.noaa.gov/cag/> (2020).
36. Barlow, J. M., Palmer, P. I., Bruhwiler, L. M. & Tans, P. Analysis of CO₂ mole fraction data: first evidence of large-scale changes in CO₂ uptake at high northern latitudes. *Atmos. Chem. Phys.* **15**, 739–745 (2015).
37. Hu, C. et al. Top-down constraints on anthropogenic CO₂ emissions within an agricultural-urban landscape. *J. Geophys. Res.-Atmos.* **123**, 4674–4694 (2018).
38. Chen, M. et al. Comparing crop growth and carbon budgets simulated across AmeriFlux agricultural sites using the Community Land Model (CLM). *Agr. Forest Meteorol.* **256**, 315–333 (2018).
39. Setiyono, T. D. et al. Understanding and modeling the effect of temperature and daylength on soybean phenology under high-yield conditions. *Field Crops Res.* **100**, 257–271 (2017).
40. Butler, E. E., Mueller, N. D. & Huybers, P. Peculiarly pleasant weather for US maize. *Proc. Natl. Acad. Sci. USA* **115**, 11935–11940 (2018).
41. Bollero, G. A., Bullock, D. G. & Hollinger, S. E. Soil temperature and planting date effects on corn yield, leaf area, and plant development. *Agron. J.* **88**, 385–390 (1996).
42. Desai, A. R. Climatic and phenological controls on coherent regional interannual variability of carbon dioxide flux in a heterogeneous landscape. *J. Geophys. Res.-Biogeophys.* **115**, G00J02 (2010).
43. Xu, B. et al. Seasonal variability of forest sensitivity to heat and drought stresses: a synthesis based on carbon fluxes from North American forest ecosystems. *Glob. Chang. Biol.* **26**, 901–918 (2020).
44. Ma, S., Osuna, J. L., Verfaillie, J. & Baldocchi, D. D. Photosynthetic responses to temperature across leaf–canopy–ecosystem scales: a 15-year study in a Californian oak-grass savanna. *Photosynth. Res.* **132**, 277–291 (2017).
45. Bond-Lamberty, B., Bailey, V. L., Chen, M., Gough, C. M. & Vargas, R. Globally rising soil heterotrophic respiration over recent decades. *Nature* **560**, 80–83 (2018).
46. Lobell, D. B. et al. Greater sensitivity to drought accompanies maize yield increase in the US Midwest. *Science* **344**, 516–519 (2014).
47. Novick, K. A. et al. The increasing importance of atmospheric demand for ecosystem water and carbon fluxes. *Nat. Clim. Chang.* **6**, 1023–1027 (2016).
48. Oren, R. et al. Survey and synthesis of intra- and interspecific variation in stomatal sensitivity to vapour pressure deficit. *Plant Cell Environ.* **22**, 1515–1526 (1999).
49. Kimm, H. et al. Redefining droughts for the US Corn Belt: the dominant role of atmospheric vapor pressure deficit over soil moisture in regulating stomatal behavior of Maize and Soybean. *Agr. Forest Meteorol.* **287**, 107930 (2020).
50. Wang, X. et al. A two-fold increase of carbon cycle sensitivity to tropical temperature variations. *Nature* **506**, 212–215 (2014).
51. Reich, P. B. et al. Effects of climate warming on photosynthesis in boreal tree species depend on soil moisture. *Nature* **562**, 263–267 (2018).
52. Hatfield, J. L. et al. Climate impacts on agriculture: implications for crop production. *Agron. J.* **103**, 351–370 (2011).
53. Ruiz-Vera, U. M., Siebers, M. H., Drag, D. W., Ort, D. R. & Bernacchi, C. J. Canopy warming caused photosynthetic acclimation and reduced seed yield in maize grown at ambient and elevated [CO₂]. *Glob. Chang. Biol.* **21**, 4237–4249 (2015).
54. Thomey, M. L., Slattery, R. A., Köhler, I. H., Bernacchi, C. J. & Ort, D. R. Yield response of field-grown soybean exposed to heat waves under current and elevated [CO₂]. *Glob. Chang. Biol.* **25**, 4352–4368 (2019).
55. Griffis, T. J. et al. Reconciling the differences between top-down and bottom-up estimates of nitrous oxide emissions for the US Corn Belt. *Glob. Biogeochem. Cycles* **27**, 746–754 (2013).
56. Wood, J. D. et al. Multiscale analyses of solar-induced fluorescence and gross primary production. *Geophys. Res. Lett.* **44**, 533–541 (2017).
57. Wuebbles, D. et al. CMIP5 climate model analyses: climate extremes in the United States. *Bull. Am. Meteorol. Soc.* **95**, 571–583 (2014).
58. Ollinger, S. V., Aber, J. D., Reich, P. B. & Freuder, R. J. Interactive effects of nitrogen deposition, tropospheric ozone, elevated CO₂ and land use history on the carbon dynamics of northern hardwood forests. *Glob. Chang. Biol.* **8**, 545–562 (2002).
59. Griffis, T. J. et al. Influence of C₄ vegetation on ¹³CO₂ discrimination and isoforcing in the upper Midwest, United States. *Glob. Biogeochem. Cycles* **24**, 4 (2010).
60. Sweeney, C. et al. No significant increase in long-term CH₄ emissions on north slope of Alaska despite significant increase in air temperature. *Geophys. Res. Lett.* **43**, 6604–6611 (2016).
61. Jeong, S. J. et al. Accelerating rates of Arctic carbon cycling revealed by long-term atmospheric CO₂ measurements. *Sci. Adv.* **4**, eaao1167 (2018).
62. Hsueh, D. Y. et al. Regional patterns of radiocarbon and fossil fuel-derived CO₂ in surface air across North America. *Geophys. Res. Lett.* **34**, L02816 (2007).
63. Berry, J. et al. A coupled model of the global cycles of carbonyl sulfide and CO₂: a possible new window on the carbon cycle. *J. Geophys. Res.* **118**, 842–852 (2013).
64. Lin, J. C. et al. A near-field tool for simulating the upstream influence of atmospheric observations: the stochastic Time-Inverted Lagrangian Transport (STILT) model. *J. Geophys. Res.-Atmos.* **108**, 4493 (2003).
65. Hausfather, Z. & Peters, G. P. Emissions—the ‘business as usual’ story is misleading. *Nature* **577**, 618–620 (2020).
66. Schwalm, C. R., Glendon, S. & Duffy, P. B. RCP8.5 tracks cumulative CO₂ emissions. *Proc. Natl. Acad. Sci. USA* **117**, 19656–19657 (2020).
67. Lobell, D. B., Field, C. B., Cahill, K. N. & Bonfils, C. Impacts of future climate change on California perennial crop yields: model projections with climate and crop uncertainties. *Agr. Forest Meteorol.* **141**, 208–218 (2006).
68. De Wit, C. T. *Simulation of Assimilation, Respiration and Transpiration of crops.* (Centre for Agricultural Publishing and Documentation, 1978).
69. Jung, M. et al. Compensatory water effects link yearly global land CO₂ sink changes to temperature. *Nature* **541**, 516–520 (2017).
70. Zeng, F. W., Collatz, G. J., Pinzon, J. E. & Ivanoff, A. Evaluating and quantifying the climate-driven interannual variability in Global Inventory Modeling and Mapping Studies (GIMMS) Normalized Difference Vegetation Index (NDVI3g) at global scales. *Remote Sens.* **5**, 3918–3950 (2013).

Acknowledgements

This research was partially supported by the United States Department of Agriculture National Institute of Food and Agriculture (USDA NIFA grant number 2018-67019-27808), the National Science Foundation (grant number 1640337), USDA Agricultural Research Service, and the Minnesota Supercomputing Institute for Advanced Computational Research.

Author contributions

T.J.G. and J.M.B. designed the research; Z.Y. analyzed data; and all authors contributed to writing of the paper.

Competing interests

The authors declare no competing interests.

Additional information

Supplementary information The online version contains supplementary material available at <https://doi.org/10.1038/s43247-021-00123-9>.

Correspondence and requests for materials should be addressed to Z.Y. or T.J.G.

Peer review information Primary handling editors: Leiya Chen, Joe Aslin

Reprints and permission information is available at <http://www.nature.com/reprints>

Publisher's note Springer Nature remains neutral with regard to jurisdictional claims in published maps and institutional affiliations.



Open Access This article is licensed under a Creative Commons Attribution 4.0 International License, which permits use, sharing, adaptation, distribution and reproduction in any medium or format, as long as you give appropriate credit to the original author(s) and the source, provide a link to the Creative Commons license, and indicate if changes were made. The images or other third party material in this article are included in the article's Creative Commons license, unless indicated otherwise in a credit line to the material. If material is not included in the article's Creative Commons license and your intended use is not permitted by statutory regulation or exceeds the permitted use, you will need to obtain permission directly from the copyright holder. To view a copy of this license, visit <http://creativecommons.org/licenses/by/4.0/>.

© The Author(s) 2021